

Article

Corrosiveness of Palm Biodiesel in Gray Cast Iron Coated by Thermoreactive Diffusion Vanadium Carbide (VC) Coating

Ariel Amaya ^{1,2}, Oscar Piamba ^{1,*}  and Jhon Olaya ¹

¹ Department of Mechanical and Mechatronics Engineering, Universidad Nacional de Colombia, Bogotá 111321, Colombia; aaamayaa@unal.edu.co (A.A.); jjolayaf@unal.edu.co (J.O.)

² Faculty of Engineering, Coordination of Mechanical Engineering, Universidad ECCL, Bogotá 111311, Colombia

* Correspondence: oepiambat@unal.edu.co; Tel.: +57-1-316-5000

Received: 13 January 2019; Accepted: 18 February 2019; Published: 20 February 2019



Abstract: Palm biodiesel is a currently used biofuel, principally as an additive or substitute of diesel fuel in vehicular internal combustion engines. In the present work, vanadium carbide (VC) coatings were deposited on gray cast iron (GCI) using the thermoreactive diffusion process (TRD) to evaluate the corrosiveness of palm biodiesel and compare it with gray cast iron corrosion behavior. VC coated and uncoated gray cast iron samples were tested by immersion corrosion tests (291 K and 313 K), cyclic oxidation test (CO), and the electrochemical impedance spectrometry test (EIS). The corrosion test showed the reduction of the corrosion rate for the VC coating when compared to gray cast iron. EIS tests of coated samples showed higher values of polarization resistance when compared with uncoated gray cast iron samples. Results confirmed that while biodiesel was more corrosive than diesel on both coated and uncoated gray cast iron, the VC coating was efficient in protecting the substrate exposed to both fuels.

Keywords: biodiesel corrosion; gray cast iron; VC coating; thermoreactive diffusion TRD

1. Introduction

Some countries have included biodiesel as an alternative energy source because it is considered as a renewable fuel, technically competitive, biodegradable, and environmentally friendly when it is compared to fossil diesel fuel [1–3]. This biofuel has been projected as a diesel substitute to use in compression ignition engines because it has fuel properties that allow its use in diesel engines without any required modifications of the engine architecture. The biodiesel is a blend of fatty acid alkyl esters produced from a large range of raw materials, such as vegetable oils, animals fats, and waste oils, principally [4,5]. It is composed of a blend of saturated and unsaturated esters and, for this reason, it has stability problems, especially because it is highly hygroscopic and sensible to temperature changes, light incidence, and the presence of metallic ions [6,7]. The unsaturated esters tend to be more reactive, promoting autoxidation, photo oxidation, and hygroscopicity processes, which cause biofuel degradation and a more corrosive process [8,9]. Due to these characteristics, biodiesel has been shown to be more corrosive than conventional diesel oil, affecting many materials that are in contact with it during its lifecycle, like polymers and metals alloys [10–12]. The wide range of raw material sources that can be used to produce biodiesel includes the palm oil tree, which stands out for its high productivity and profitability in tropical areas, such as Indonesia, Malaysia, and Colombia [13,14].

The literature shows that the corrosive behavior of biodiesel produced from many kinds of feedstock, principally canola, soybean, sunflower, and palm oil, has been evaluated. The most utilized

corrosion test is the method of corrosiveness to copper strip, based on ASTM 130-12 [15], which has allowed the identification that biodiesel is more corrosive than diesel [16]. Research on corrosion immersion tests has been ongoing during the last decade, evaluating effects of biofuels from different raw materials on metal alloys, polymers, and other materials used in the automotive and chemical processes industries. Tests made on copper samples and low carbon steel immersed in rapeseed biodiesel at 48 °C reveal that biodiesel causes deterioration of the samples and these effects increase when the biofuel degrades, forming organic salts and metallic oxides, or when it absorbs moisture from its surroundings [17]. Materials, such as bronze, copper, steel, and aluminum, were tested in biodiesel, presenting corrosion effects and forming sediments, which increased the ionic conductivity of biofuel [18,19]. The influence of temperature and exposure time on the corrosion effects of palm biodiesel in 1045 carbon steel were also evaluated, observing that the increase of temperature promotes the oxidation-reduction reactions and long periods of exposure time allow a higher degradation state of biofuel, increasing the corrosive effects and making the damages by pitting more visible [20,21]. Corrosion immersion testing of biodiesel on gray cast iron showed that an increase of the temperature in the test affects the corrosion velocity, and that the iodine value (IV) of biodiesel is also related with corrosion effects, as highly unsaturated esters are more corrosive [22]. The presence of iron oxides was also identified by x-ray diffraction (FeO and Fe₂O₃) on a cast iron surface exposed to palm biodiesel [23]. Electrochemical impedance spectroscopy (EIS) has also been used to evaluate the corrosiveness of biodiesel on materials in automotive parts. This test allows the identification of the biodiesel raw materials that influence the polarization resistance [24]. An alternative EIS methodology was developed to evaluate the corrosion behavior of soybean biodiesel. This methodology used an electrochemical cell without support electrolytes and was tested on four kinds of materials. Results showed that this methodology is capable of measuring the corrosiveness of biodiesel. These results also allowed a conclusion regarding which electrochemical techniques are a fast and efficient test method to measure the corrosion effects of biodiesel [25]. The corrosiveness of palm biodiesel on gray iron has been studied, and the results show that the corrosion rate is three times higher for biodiesel than diesel and that the polarization resistance decreases when diesel is substituted by biodiesel [26].

The application of coatings is a useful technique to protect materials when corrosion environments are present. The processes used to grow these coatings to an industrial scale are, among others, physical vapor deposition (PVD) and chemical vapor deposition (CVD) [27], which both have advantages and disadvantages. For example, both processes need expensive and complex equipment that must be operated under high-vacuum conditions. The thermal-CVD process is performed at high temperatures (700–1200 °C) while the PVD process can be performed at lower temperatures, but due to the reduced amount of diffusion during the film deposition, the adhesion of the coatings can be weak [27]. Other techniques to produce hard coatings are the plasma thermal spray and high velocity oil fuel (HVOF). Both techniques are expensive and the coatings produced can have a high porosity and porosity with oxides. Another option for the production of coatings or hard coatings is the thermo-reactive deposition process (TRD). The advantages of the TRD process include its low cost, because the treatment is performed at atmospheric pressure and it does not require any expensive equipment [27]. The TRD process in a borax bath has been efficiently used to obtain hard layers of carbide with a high corrosion resistance on substrates with a carbon content above 0.3 wt%. This process allows the production of binary or ternary coatings that improve the surface properties, and can be produced at lower cost [28,29]. These hard carbide layers exhibit a low friction coefficient and good anticorrosive properties, with thicknesses ranging between 5 and 15 microns, depending on the carbon content of the substrate, the temperature, and the time of the treatment [30]. The range of deposition temperatures is between 1123 and 1323 K, and the immersion time ranges from 0.5 to 10 h. In TRD, the part to be coated is immersed in a bath of borax deca-hydrate, which loses its binding water at the treatment temperature (Na₂B₄O₇ • 10H₂O). In addition, the carbide forming element (CFE) for the case under study of vanadium ferroalloy is previously dissolved in the bath. These compounds react chemically with the carbon atoms diffusing from the substrate to the surface, forming a new layer on the interface

based on the carbide-forming element selected [30]. The mechanism of diffusion among the Fe (steel) and the transition metal allow excellent adhesion of the coating/substrate system.

Previous studies on the use of hard coatings to protect gray iron have been developed by applying niobium carbide coatings using the thermo reactive process [31]. This research confirmed that gray cast iron is more susceptible to corrosion attack by biodiesel than by diesel, being three times higher when cyclic oxidation is developed, and that niobium carbide coatings reduce the corrosion rate of biodiesel up to the diesel reference level. The polarization resistance measured by EIS at 1, 24, 48, and 144 h also shows the same behavior, and allows the conclusion that niobium carbide coatings act as a protection against corrosion by palm biodiesel. Vanadium carbide coatings applied on iron alloys show an improvement in corrosion resistance and hardness in saline (0.3% NaCl) environments at room temperature [32] and are considered as an option to improve the corrosion resistance of gray iron mechanical parts when they are in contact with biodiesel.

Diesel engines are designed to run using distilled petroleum fuel. The substitution or addition of alternative fuel modifies the fuel chemical composition and, consequently, its corrosive effects on engine materials. This research is focused on studying the effectiveness of a vanadium carbide coating as a corrosion protector of gray cast iron when it is in contact with palm biodiesel. To analyze the coating behavior under biodiesel attack, static immersion and electrochemical impedance spectroscopy tests are used. Coated and uncoated samples of gray cast iron are analyzed by SEM-FEG and DRX after the corrosion test. Results are compared to evaluate the advantages of using thermoreactive vanadium carbide coating as a biodiesel corrosion protector.

2. Materials and Methods

To develop this research, two kinds of fuels were used: Low sulfur diesel (less than 500 ppm sulphur) and palm biodiesel (palm oil methyl ester) produced by transesterification via alkali. The diesel is a fuel produced from petroleum, by distillation between 230 and 320 °C, and composed principally by alkanes, with hydrocarbon chains from 14 to 20 carbon atoms long. The biodiesel is oxygenated biofuel produced by chemical transformation of triglycerides from a biological source, like vegetable oil or animal tallow. The composition of biodiesel was analyzed by gas chromatography [33], resulting in a concentration of 42.5% methyl ester palmitate, 40.7% methyl ester oleate, 10% methyl ester linoleate, 4.9% methyl ester stearate, and 1.9% methyl ester myristate. Total unsaturated esters were 50.7%. Reports of diesel and biodiesel properties measured according to ASTM D6751-15c [34] were supplied by the manufacturers and are shown in Table 1.

Table 1. Diesel and Palm biodiesel properties.

Tests	Units	Diesel	Biodiesel
Density at 15 °C	Kg/m ³	857	879
Viscosity at 40 °C	mm ² /s	4,68	4.46
Flashpoint	°C	82	271
Cetane number	-	48	74.1
Total ester content	%(m/m)	-	98.8
Moisture	mg/kg	500	497
Methanol content	%(m/m)	-	0.18
Total glycerol	%(m/m)	-	0.22

Samples of gray cast iron were obtained from an unused cylinder liner available from a diesel engine. The material was cataloged as a G3500 grey iron (93.1% Fe, 3.45% C, 1.66% Si, 0.66% Mn, 0.2% S and impurities), density 7.21 g/cm³, and of pearlite structure, which show randomly distributed lamellar graphite. Square samples of a 2 cm width and 0.5 cm thickness were cut, polished to remove scratches, and cleaned. Vanadium carbide coatings were deposited on the samples by TRD in a borax salt bath 81%wt, ferro-vanadium (16%) and aluminum (3%), following a methodology reported by Amaya et al. [30], at 1273 K for 4 h. The morphology of VC coatings was characterized

using a Field Emission Gun Scanning Electron Microscopy (SEM-FEG) Microscope, the Tescan-Mira3 (Brno–Kohoutovice, Czech Republic), at 1×10^{-7} torr, 30 kV for the coating surface and 15 kV for the transversal section. A micrographic at $20000\times$ of the coating surface is shown in Figure 1a, which exhibits a clearly equiaxial morphology, with the size of the grains between 0.2 and 0.6 μm , and randomly distributed pores, and homogeneous growth throughout the surface. The transversal section micrographic, Figure 1b, exhibits a planar interface substrate-coating, with an average thickness coating of approximately 10 μm , measured using a 500 Optical Microscope (LECO Corporation, St. Joseph, MI, USA), showing the presence of pores in the coating that are randomly and have a medium size of 1 μm . Pore formation is a consequence of grain growth in the TRD process. These defects allow the passage of the electrolyte from the surface to the interface reducing the corrosion resistance of the coating. The coating was analyzed by Auger Electron Scattering (AES) using an Omicron Nanotechnology CMA 169 (Oxford Instruments, Abingdon, UK), with an evaluation range between 100 and 500 eV with a 0.5 eV resolution. The results obtained from AES testing were analyzed using the database of the National Institute of Standards and Technology (NIST). The presence of mainly vanadium (431, 437, and 473 eV) and carbon (272 eV) was verified. The analysis of the material concentrations showed 44.78% carbon and 55.22% vanadium.

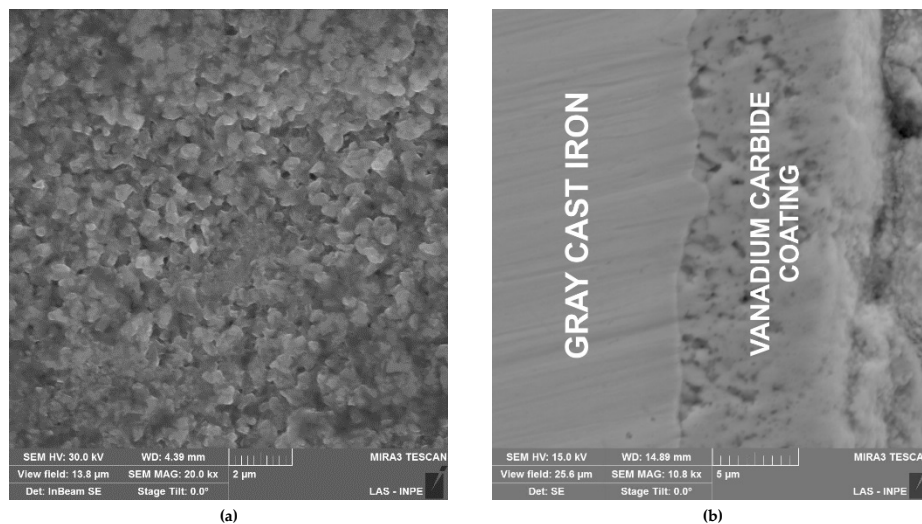


Figure 1. SEM micrograph: (a) Surface of vanadium carbide $20,000\times$ and (b) a cross section of coating $10,800\times$.

The corrosive effects of biodiesel in gray cast iron were evaluated by immersion testing at 291 and 313 K, in each fuel. Three samples per treatment were tested, for 1320 h (55 days). Static immersion tests were carried out using opaque and hermetic containers, fulfilled of fuel. Cyclic oxidation tests were also performed for a total time of 1320 h (55 days). Each cycle lasted 1.5 h and was repeated to complete the total test time. The cycle included 0.25 h of heating, 0.75 h at 473 K, 0.25 h of cooling, and 0.25 h at 291 K. When the time of the test was finished, the samples were cleaned with a solution of hydrochloric acid and TiN chloride in an ultrasound bath at room temperature. Mass was measured using the Sartorius Bp211D (Sartorius AG, Goettingen, Germany) analytical balance, and weight loss was measured following the ASTM G31-12 [35]. The corrosion rate of each treatment was calculated in mils per year (0.001 inches per year, mpy) using Equation (1):

$$\text{Corrosion Rate [mpy]} = (W[\text{g}] \times 3.45 \times 10^6) / (A[\text{cm}^2] \times \rho[\text{g/cm}^3] \times t[\text{h}]) \quad (1)$$

W is the weight loss (g); 3.45×10^6 is a unit conversion factor; ρ is the density (g/cm^3); A is the exposed surface (cm^2); and t is the test time (h) [35,36].

After the immersion test was completed, the morphology of the samples of gray cast iron and VC coating were characterized using high vacuum pressure SEM-FEG Microscopy, in a Tescan-Mira3

(Brno–Kohoutovice, Czech Republic), at 1×10^{-7} torr and 30 kV. X-ray Diffraction (XRD) studies were performed on tested samples to identify the effects of the corrosive process on the microstructure of the VC coating. Diffractograms were obtained using a high power X'Pert PRO system (Panalytical, Almelo, The Netherlands), at 45 kV and 40 mA, with a 1.594 \AA $\text{CuK}\alpha$ monochromatic source, and a 2θ range between 35° and 100° , and a 0.02° resolution.

To complement the immersion test, electrochemical impedance spectroscopy (EIS) tests were performed for samples of bare gray cast iron and VC coatings, in the presence of diesel and biodiesel. EIS tests were performed for 144 h at $291 \pm 2 \text{ K}$, using a Gamry–Reference 600 (Gamry Instruments, Inc., Philadelphia, PA, USA). A three-electrode electrochemical cell was used. The cell is formed by two 4 cm^2 parallel surfaces that function as the working and auxiliary electrode, the specimen holder, and a high-density graphite, respectively. The reference electrode was a 0.5 mm diameter silver wire (Ag). The distance from the sample to the reference electrode was 0.75 mm and the distance from the sample to the auxiliary electrode was 1.5 mm, with the exposed sample area being 78.54 mm^2 . The signal amplitude used was 200 mV and the frequency range was between 0.00001–100 kHz. The test signals were acquired with the EIS300 module and analyzed using Echem Analyst software (Gamry Instruments, Inc., Philadelphia, PA, USA).

3. Results and Discussion

The corrosion rates of diesel and biodiesel in VC coated and uncoated gray cast iron at three temperature immersion treatments are shown in Figure 2. The figure shows that the corrosion rates of biodiesel on GCI are higher than diesel on GCI, for all conditions tested. It is also observed that the corrosion rates of biodiesel on coated samples are lower than the GCI specimens. At room temperature (291 K), a higher corrosion rate was measured for the biodiesel–GCI couple, and it was nine times higher than the diesel–GCI rate. The lowest corrosion rate appeared in the diesel–VC coating sample array, while the biodiesel–GCI array exhibited a corrosion rate eight times higher. The corrosion rate of biodiesel on the vanadium carbide coating was 36% lower than the biodiesel–GCI corrosion rate. The high temperature test caused an increase in the corrosion rates. This behavior is greater for the GCI than the VC coating samples. When the tests were performed at 313 K, the corrosion rate increased, with the biodiesel–gray cast couple having the highest rate, which confirms the protection behavior of the VC coating, since it reduced the corrosion rate by 40%. The cyclic oxidation test increased the corrosion rate at a greater scale. The highest corrosion rate was observed by biodiesel in gray cast iron and was reduced by 45% when the VC coat was used. The VC coat also showed better behavior on diesel when a cyclic oxidation treatment was applied.

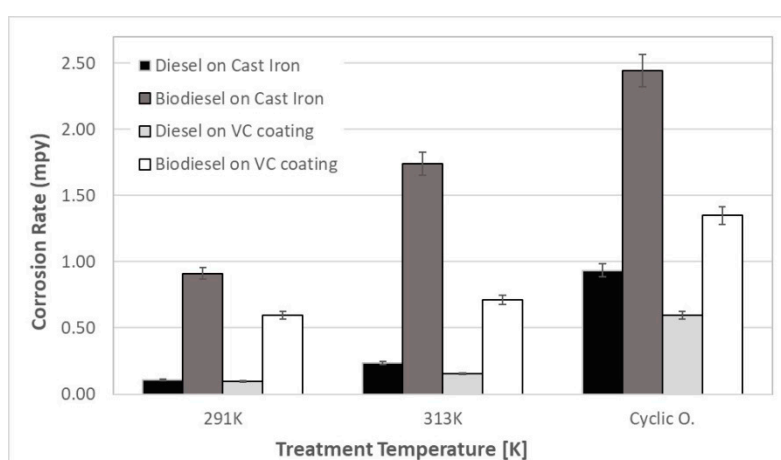


Figure 2. Corrosion rates of the gray cast iron and VC coating in diesel and biodiesel.

Figure 3 shows the $1000\times$ SEM micrographics of gray cast iron and VC coatings samples after treatment in biodiesel for 1320 h, under cyclic oxidation conditions. In Figure 3a, GCI exhibits surface

pitting, approximately 50 μm in size, which was distributed randomly on the sample surface. This GCI surface damage could originate from partial loss of the lamellar graphite, causing grooves that thus promoted the selective corrosion process in ferrite. Figure 3b shows the morphology of the oxidized VC coating, presenting a smaller size of approximately 4 μm and low depth aleatory pitting, when compared to the GCI treatment. Figure 4 shows a 15,000 \times SEM micrographic that details the morphology of pitting in the vanadium carbide surface, allowing us to identify the low growth of intergranular oxides.

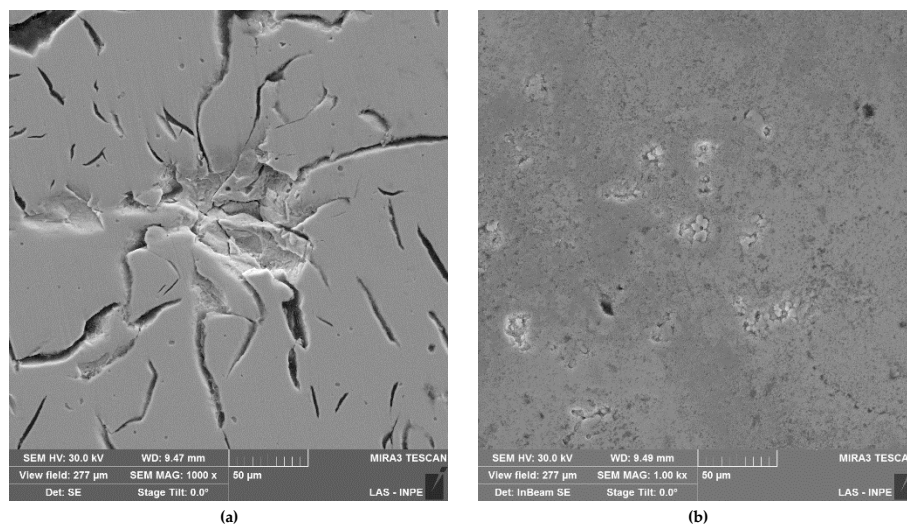


Figure 3. SEM–FEG micrograph on the surface exposed to palm biodiesel at 1320 h. (a) Gray cast iron and (b) VC coating.

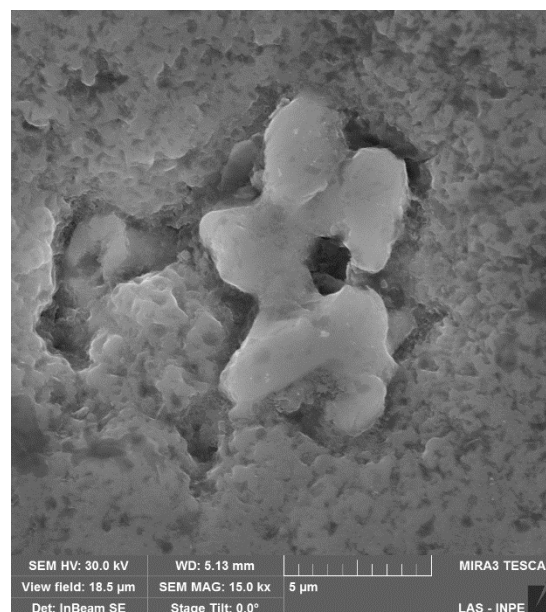


Figure 4. SEM–FEG micrograph of VC coating exposed to palm biodiesel at 1320 h.

Figure 5 shows diffractograms of vanadium carbide before and after the corrosion treatment in biodiesel. XRD analysis allows the identification of the cubic phase of V_8C_7 , represented by the crystalline planes, (222), (400), (440), and (622), principally, according to the JCPDS-00-038-1364 chart. Analyses developed in oxidized samples allow the identification of two types of oxides, V_2O_5 and V_3O_5 , in accordance with JCPDS 01-071-0039 and JCPDS 00-054-0513, respectively. The presence of additional peaks related to V_2O_5 and V_3O_5 showed that the VC surface interacted with the biodiesel and diesel,

and that these species of oxides were produced during the corrosion process. The observed peaks showing low intensities (between 0.3% and 0.5%), i.e., the peak of V_2O_5 (872), are more representative. These results revealed the low growth of crystalline oxides on the VC surface.

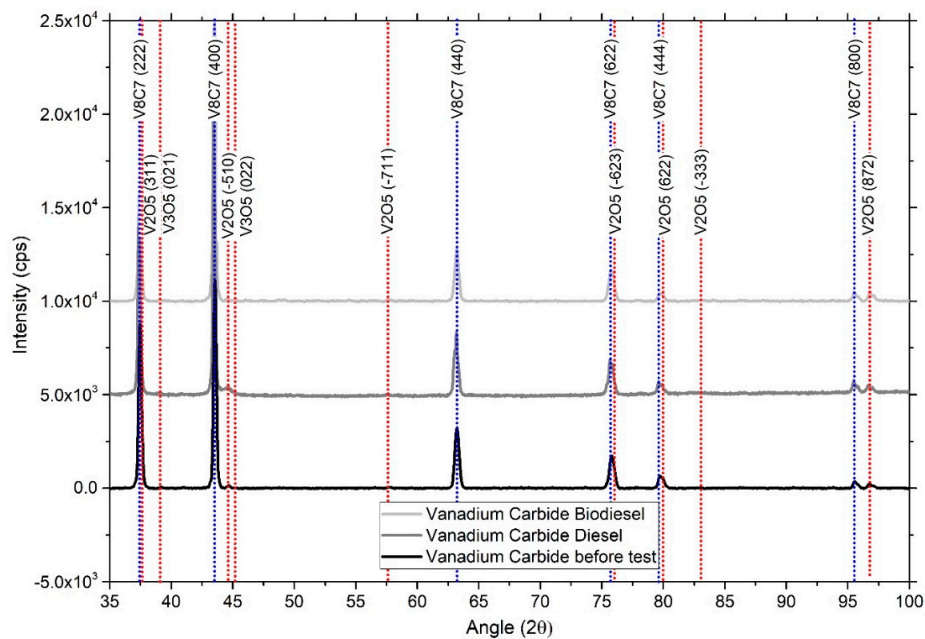


Figure 5. XRD spectrum of the VC coating before and after exposure to palm biodiesel at 1320 h in cyclic oxidation.

Figure 6 shows the results of electrochemical impedance spectroscopy analyses applied to VC coating samples at 291 ± 2 K for four test times. Results are shown in a Nyquist diagram. Each diagram is composed of two semicircles; at low frequencies, the larger semicircle is related to the resistive-capacitive characteristic of a porous coating, and at high frequencies, the small semicircle is associated with the resistive-capacitive behavior of the Helmholtz double layer [23,30]. The polarization resistance changed for each test time, evidencing the corrosive effects in the coating. The average polarization resistance increased during the first 24 h of testing to a maximum ($9.86 \times 10^9 \Omega$). For higher times, the polarization resistance decreases, showing a lower value at 144 h of test time ($8.26 \times 10^9 \Omega$).

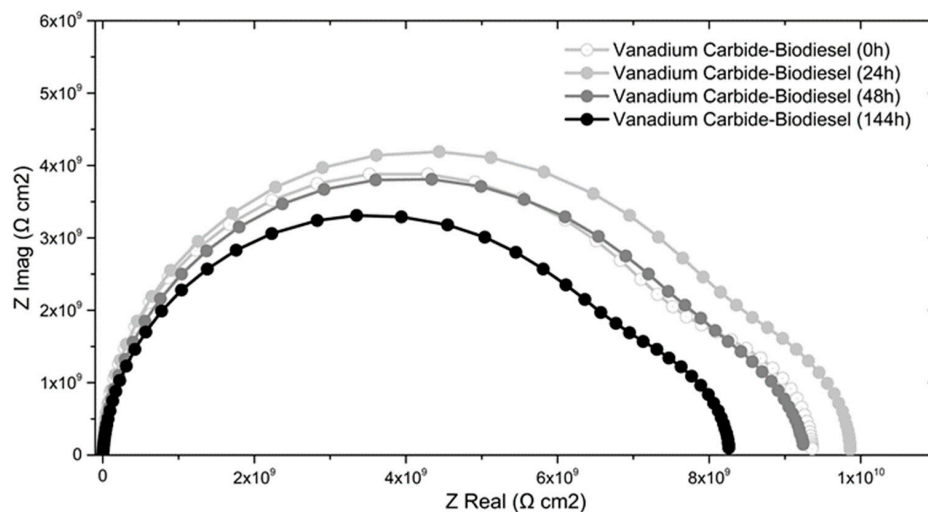


Figure 6. Nyquist diagrams obtained via EIS on the VC coating in contact with palm biodiesel at 291 ± 2 K at different exposure times.

Nyquist diagrams in Figure 7 allow a comparison of the corrosion behavior of diesel and biodiesel in the GCI and VC coating at 144 h of treatment time to be made. The Nyquist diagrams of diesel and biodiesel in gray iron exhibit a semicircle shape, according to the resistive-capacitive behavior of the double layer reported by Mpeko [24] and Amaya [26]. It is observed that the polarization resistance of diesel and biodiesel on the vanadium carbide coating is higher than that shown by both fuels in GCI and improves the polarization resistance of the conventional array “diesel-gray cast iron”. Figure 8 shows the polarization resistance behavior for four testing times, 1, 24, 48, and 144 h. It can be observed that the coated samples have a higher polarization resistance than the gray cast iron samples, showing better behavior than the diesel-gray cast iron configuration, which was used as the reference. The coating exhibited similar behaviors for the two fuels tested, while the iron casting behaved differently in response to the two fuels. The values of the polarization resistance in Figure 7 confirmed that the VC coating has better behaviors, irrelevant of the fuel type. The results allow us to conclude that the electrochemical impedance spectroscopy can be applied to measure the corrosive behavior in diesel and biodiesel. The test conditions allowed us to overcome the fuel resistance and to measure the fuel-surface electrochemical interaction, without the use of support electrolytes [25].

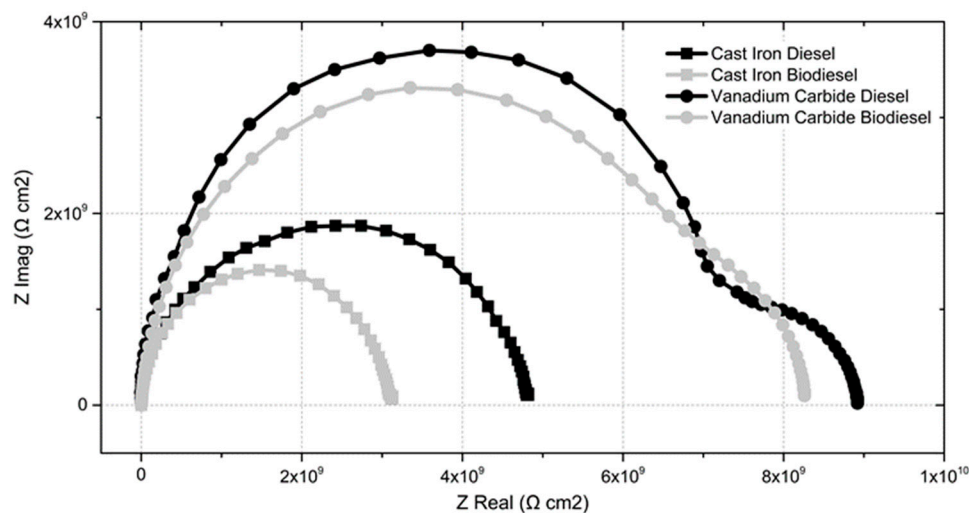


Figure 7. Nyquist diagrams obtained via EIS for the gray cast iron and vanadium carbide coating in contact with diesel and palm biodiesel at 291 ± 2 K for 144 h.

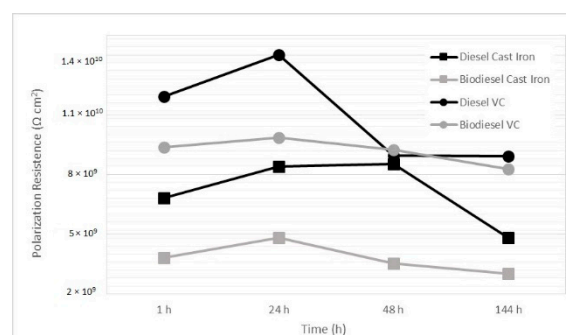


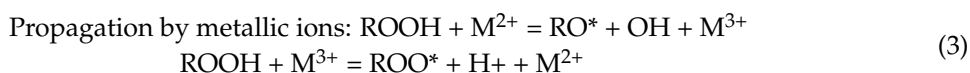
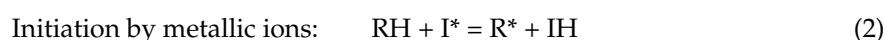
Figure 8. Polarization resistance obtained from the Nyquist diagrams via EIS on the gray cast iron and VC coating for 1, 24, 48, and 144 h, at 291 ± 2 K.

The results of the corrosion rate and polarization resistance, obtained from the immersion corrosion test and electrochemical test, showed that the vanadium carbide coating produced by the TRD process improved the corrosion resistance of the gray cast iron when it was in contact with palm biodiesel. When the gray cast iron was tested, the polarization resistance of biodiesel was lower than the diesel treatment, corresponding to the corrosive behavior on gray cast iron obtained in the

immersion test. The vanadium carbide coating exhibited better behavior than GCI, for the two fuels tested. The Nyquist diagrams confirm the results obtained by the corrosion rate test, by the static immersion and cyclic oxidation tests.

These results can be compared with previous research about the corrosiveness effects of palm biodiesel in gray cast iron and niobium carbide coatings [30]. Morphologic analyses of corrosion effects on coating samples show that both carbides suffer from pitting, however, damage is higher in vanadium carbide. Quantitative comparisons can be performed using the corrosion test values. Corrosion rates of biodiesel in vanadium carbides were higher than niobium carbide, but lower than those that occurred in the gray cast iron. Similar results were observed when the polarization resistance was compared. XRD analyses also identified the oxides that formed on the coated surfaces after the corrosion test, which begin in the intergranular borders and initiated the pitting process. Biodiesel autooxidation processes degrade the fuel and produce aldehydes, carboxylic acids, alcohols, sediments, and insoluble gums [37]. Pitting on the surface is the effect of oxidizing acids, especially, acting on vanadium and niobium carbide and dissolving the carbides [38].

Biodiesel is composed of esters of fatty acids, with the presence of unsaturated carbon-carbon double bonds, two oxygen atoms, and hydrogen. This composition promotes the autoxidative process, where the oxygen attacks the double bond to produce peroxides [6,39]. The autoxidative process involves the attack of an initiator radical that removes one hydrogen from a carbon atom to produce a carbon free radical. The metallic ion can be the initiator radical (I^*). Metallic ions also act as the catalyzer in secondary stages (M^{2+} , M^{3+}), where peroxides react to produce peroxide radicals and hydrogen ions, which reacts further to promote the oxidation process. Metallic ions also favor the formation of secondary oxidation products, such as acids, aldehydes, free fatty acids, and polymers [40,41]. The mechanisms are shown in Equations (2) and (3):



The products of the autoxidation of biodiesel are corrosive in metallic materials. They induce the formation of oxides and the release of metal ions from the surface that favor the continuity of the autoxidative cycle in the array. These effects can be observed in the results of the immersion corrosion test of the gray cast iron in palm biodiesel, in which the formation of oxides on the surface and pitting in the ferrite phase show the corrosive activity of the electrolyte. This process is favored by the presence of unsaturated bonds in biodiesel, as identified by Castro [22], and by the temperature of the test, as shown in Figure 2. The vanadium carbide coating is a ceramic material characterized as inert and it has large bonding energies. These coatings' attributes improve the response to corrosion by biodiesel autooxidation products and they inhibit the release of metallic ions that promote biodiesel autoxidative processes, as can be deduced from Figures 3 and 5. Some studies have found that the corrosion resistance of vanadium carbide in the presence of acids can be reduced, for example, in the presence of H_2SO_4 , the VC can be dissolved and produce vanadyl sulfate hydrate ($\text{VO}_2\text{SO}_4 \cdot \text{H}_2\text{O}$) [42]. However, the results of X-ray diffraction did not show the presence of this corrosion product, in opposition to the presence of vanadium oxides that slightly affected the corrosion resistance of the coating.

In summary, the corrosion rate measured for the vanadium carbide coating test was, on average, 40% lower than the corrosion rate of biodiesel in gray cast iron. The polarization resistance of biodiesel-VC samples was 2.5 times higher than the biodiesel-GCI array, and for all times of exposure, it was higher than the polarization resistance measured for the reference treatment: Diesel-GCI. These results show that the VC coating can be considered a good alternative to protect the gray cast iron of palm biodiesel corrosion, however, its protector behavior is lower than niobium carbide coating.

4. Conclusions

Corrosion immersion testing allows the conclusion that vanadium carbide coating protects gray cast iron against corrosion by biodiesel. Corrosion rates of biodiesel on carbide coating were 50% lower than gray cast iron. Biodiesel corrodes the samples, causing pitting, but the damage is greater in gray cast iron samples. Morphology and crystallography analyses allowed us to conclude that vanadium oxides form on the surface coatings, principally V_2O_5 and V_3O_5 . Electrochemical tests showed that the polarization resistance was 2.5 times higher for coated samples, which reinforces the results obtained by immersion tests, ratifying the protective behavior of vanadium carbide coatings.

Author Contributions: O.P. and J.O. conceived and designed the experiments; A.A. performed the experiments; and O.P., J.O. and A.A. wrote the paper.

Funding: This research was funded by Universidad Nacional de Colombia, Research Division Bogotá, [19070],[14230].

Conflicts of Interest: The authors declare no conflict of interest.

References

1. Knothe, G. Chapter 2. History of Vegetable Oil-Based Diesel Fuels. In *The Biodiesel Handbook*, 2nd ed.; Knothe, G., Krahl, J., Gerpen, J., Eds.; Academic Press and AOCS Press: Urbana, IL, USA, 2010; pp. 5–19, ISBN 9780983507260. [CrossRef]
2. Basha, S.A.; Raja Gopal, K.; Jebaraj, S. A review on biodiesel production, combustion, emissions and performance. *Renew. Sust. Energy Rev.* **2009**, *13*, 1628–1634. [CrossRef]
3. Ashraful, A.M.; Masjuki, H.H.; Kalam, M.A.; Fattah, I.R.; Imtenan, S.; Shahir, S.A.; Mobarak, H.M. Production and comparison of fuel properties, engine performance, and emission characteristics of biodiesel from various non-edible vegetable oils: A review. *Energy Convers. Manag.* **2014**, *80*, 202–228. [CrossRef]
4. Moser, B.R. Biodiesel Production, Properties, and Feedstocks. *In Vitro Cell. Dev. Biol. Plant.* **2009**, *45*, 229–266. [CrossRef]
5. Singh, S.P.; Singh, D. Biodiesel production through the use of different sources and characterization of oils and their esters as the substitute of diesel: A review. *Renew. Sust. Energy Rev.* **2010**, *14*, 200–216. [CrossRef]
6. Knothe, G. Some aspects of biodiesel oxidative stability. *Fuel Process. Technol.* **2007**, *88*, 669–677. [CrossRef]
7. Knothe, G. “Designer” Biodiesel: Optimizing Fatty Ester Composition to Improve Fuel Properties. *Energy Fuels* **2008**, *22*, 1358–1364. [CrossRef]
8. Knothe, G. Dependence of biodiesel fuel properties on the structure of fatty acid alkyl esters. *Fuel Process. Technol.* **2005**, *86*, 1059–1070. [CrossRef]
9. Kaul, S.; Saxena, R.C.; Kumar, A.; Negi, M.S.; Bhatnagar, A.K.; Goyal, H.B.; Gupta, A.K. Corrosion behavior of biodiesel from seed oils of Indian origin on diesel engine parts. *Fuel Process. Technol.* **2007**, *88*, 303–307. [CrossRef]
10. Fazal, M.A.; Haseeb, A.S.M.A.; Masjuki, H.H. Biodiesel feasibility study: An evaluation of material compatibility; performance; emission and engine durability. *Renew. Sustain. Energy Rev.* **2010**, *15*, 1314–1324. [CrossRef]
11. Singh, B.; Korstad, J.; Sharma, Y.C. A critical review on corrosion of compression ignition (CI) engine parts by biodiesel and biodiesel blends and its inhibition. *Renew. Sustain. Energy Rev.* **2012**, *16*, 3401–3408. [CrossRef]
12. Fazal, M.A.; Haseeb, A.S.M.A.; Masjuki, H.H. Degradation of automotive materials in palm biodiesel. *Energy* **2012**, *40*, 76–83. [CrossRef]
13. Kalam, M.A.; Masjuki, H.H. Biodiesel from palm oil—An analysis of its properties and potential. *Biomass Bioenergy* **2002**, *23*, 471–479. [CrossRef]
14. USDA. Oilseeds: World Markets and Trade. Available online: <https://www.fas.usda.gov/data/oilseeds-world-markets-and-trade> (accessed on 10 January 2019).
15. ASTM D130-18. *Standard Test Method for Corrosiveness to Copper from Petroleum Products by Copper Strip Test*; American Society for Testing and Materials: West Conshohocken, PA, USA, 2018.
16. Knothe, G. Chapter 5. Analytical Methods. In *The Biodiesel Handbook*, 2nd ed.; Knothe, G., Krahl, J., Gerpen, J., Eds.; Academic Press and AOCS Press: Urbana, IL, USA, 2010; pp. 97–130. ISBN 9780983507260. [CrossRef]

17. Hu, E.; Xu, Y.; Hu, X.; Pan, L.; Jiang, S. Corrosion behaviors of metals in biodiesel from rapeseed oil and methanol. *Renew. Energy* **2012**, *37*, 371–378. [[CrossRef](#)]
18. Fazal, M.A.; Haseeb, A.S.M.A.; Masjuki, H.H. Comparative corrosive characteristics of petroleum diesel and palm biodiesel for automotive materials. *Fuel Process. Technol.* **2010**, *91*, 1308–1315. [[CrossRef](#)]
19. Maru, M.; Lucchese, M.; Legnani, C.; Quirino, W.; Balbo, A.; Aranha, I.; Costa, L.; Vilani, S.; Sena, L.; Damasceno, J. Biodiesel compatibility with carbon steel and HDPE parts. *Fuel Process. Technol.* **2009**, *90*, 1175–1182. [[CrossRef](#)]
20. Jin, D.; Zhou, X.; Wu, P.; Jiang, L.; Ge, H. Corrosion behavior of ASTM 1045 mild steel in palm biodiesel. *Renew. Energy* **2015**, *81*, 457–463. [[CrossRef](#)]
21. Fazal, M.A.; Haseeb, A.S.M.A.; Masjuki, H.H. Effect of temperature on the corrosion behavior of mild steel upon exposure to palm biodiesel. *Energy* **2011**, *36*, 3328–3334. [[CrossRef](#)]
22. Castro, J.; Piamba, O.E.; Olaya, J.J. Pruebas de corrosión cíclica de fundiciones de hierro gris en diferentes biodiesel. *Tecnol. Desarro.* **2016**, *5*, 423–429.
23. Fazal, M.A.; Haseeb, A.S.M.A.; Masjuki, H.H. Effect of different corrosion inhibitors on the corrosion of cast iron in palm biodiesel. *Fuel Process. Technol.* **2011**, *92*, 2154–2159. [[CrossRef](#)]
24. M'Peko, J.C.; Reis, D.L.S.; De Souza, J.E.; Caires, A.R.L. Evaluation of the dielectric properties of biodiesel fuels produced from different vegetable oil feedstocks through electrochemical impedance spectroscopy. *Int. J. Hydrog. Energy* **2013**, *38*, 9355–9359. [[CrossRef](#)]
25. Aquino, I.P. Avaliação da Corrosividade do Biodiesel por Técnicas Gravimétricas e Electroquímicas. Ph.D. Thesis, Universidade de São Paulo, São Paulo, Brasil, 2012.
26. Amaya, A.A.; Piamba, O.E.; Olaya, J.J. Study of the corrosive effects of diesel and biodiesel on gray cast iron. *Rev. Lat. Metal. Mater.* **2014**, *34*, 289–295.
27. Castillejo, F.E.; Marulanda, D.M.; Olaya, J.J.; Alfonso, J.E. Wear and corrosion resistance of niobium–chromium carbide coatings on AISI D2 produced through TRD. *Surf. Coat. Technol.* **2014**, *254*, 104–111. [[CrossRef](#)]
28. Arai, T.J. Carbide coating process by use of molten borax bath in Japan. *Heat Treat.* **1979**, *1*, 15. [[CrossRef](#)]
29. Fan, S.; Yang, Z.; Zhang, C.; Zhang, D.; Che, H. Evaluation of vanadium carbide coatings on AISI H13 obtained by thermo-reactive deposition/diffusion technique. *Surf. Coat. Technol.* **2010**, *205*, 641–646. [[CrossRef](#)]
30. Amaya, A.; Piamba, O.; Olaya, J. Vanadium carbide coatings produced on gray cast iron using the thermo-reactive deposition/diffusion technique. *Ing. Mec. Technol. Des.* **2015**, *5*, 333–338.
31. Amaya, A.; Piamba, O.; Olaya, J. Improvement of Corrosion Resistance for Gray Cast Iron in Palm Biodiesel Application Using Thermoreactive Diffusion Niobium Carbide (NbC) Coating. *Coatings* **2018**, *8*, 216. [[CrossRef](#)]
32. Aguzzoli, C.; Figueroa, C.A.; de Souza, F.S.; Spinelli, A.; Baumvol, I.J.R. Corrosion and nanomechanical properties of vanadium carbide thin film coatings of tool steel. *Surf. Coat. Technol.* **2012**, *206*, 2725–2731. [[CrossRef](#)]
33. Narvaez, P.C.; Torres, J.A.; Sanchez, F.; de Leon, L.F. Determinación por cromatografía de gases de alquil ésteres (metílico y etílico) de ácidos grasos, en presencia de mono-, di-, y triglicéridos. *Ing. E Investig.* **2005**, *57*, 58–62.
34. ASTM. *D6751-15c Standard Specification for Biodiesel Fuel Blend Stock (B100) for Middle Distillate Fuels*; ASTM International: West Conshohocken, PA, USA, 2004.
35. ASTM. *G31-72 Standard Practice for Laboratory Immersion Corrosion Testing of Metals*; ASTM International: West Conshohocken, PA, USA, 2004.
36. Babolan, R. *Corrosion Tests and Standards: Application and Interpretation*, 2nd ed.; ASTM International: West Conshohocken, PA, USA, 2005; p. 882.
37. Sundus, F.; Fazal, M.A.; Masjuki, H.H. Tribology with biodiesel: A study on enhancing biodiesel stability and its fuel properties. *Renew. Sustain. Energy Rev.* **2017**, *70*, 399–412. [[CrossRef](#)]
38. Pierson, H.O. Chapter 5—Carbides of Group V: Vanadium, Niobium and Tantalum Carbides. In *Handbook of Refractory Carbides and Nitrides; Properties, Characteristics, Processing and Applications*; Pierson, H.O., Ed.; Noyes Publications: Westwood, NJ, USA, 1996; pp. 89–97. ISBN 978-0-8155-1392-6.
39. Fazal, M.A.; Jakeria, M.R.; Haseeb, A.S.M.A. Effect of copper and mild steel on the stability of palm biodiesel properties: A comparative study. *Ind. Crop. Prod.* **2014**, *58*, 8–14. [[CrossRef](#)]

40. Jakeria, M.R.; Fazal, M.A.; Haseeb, A.S.M.A. Influence of different factors on the stability of biodiesel: A review. *Renew. Sust. Energy Rev.* **2014**, *30*, 154–163. [[CrossRef](#)]
41. Kumar, N. Oxidative stability of biodiesel: Causes, effects and prevention. *Fuel* **2017**, *190*, 328–350. [[CrossRef](#)]
42. Konadua, D.S.; Van der Merwea, J.; Potgieterb, J.H.; Potgieter-Vermaak, S.; Machio, C.N. The corrosion behaviour of WC-VC-Co hardmetals in acidic media. *Corros. Sci.* **2010**, *52*, 3118–3125. [[CrossRef](#)]



© 2019 by the authors. Licensee MDPI, Basel, Switzerland. This article is an open access article distributed under the terms and conditions of the Creative Commons Attribution (CC BY) license (<http://creativecommons.org/licenses/by/4.0/>).